Bounds on Heavy Axions with an X-Ray Free Electron Laser

Jack W. D. Halliday,[1,2,3] Giacomo Marocco,[4] Konstantin A. Beyer,[1,5] Charles Heaton,[1] Motoaki Nakatsutsumi,[6] Thomas R. Preston,[6] Charles D. Arrowsmith,[1] Carsten Baehtz,[7] Sebastian Goede,[6] Oliver Humphries,[6] Alejandro Laso Garcia,[7] Richard Plackett,[1] Pontus Svensson,[1] Georgios Vacalis,[1] Justin Wark,[1] Daniel Wood,[1] Ulf Zastrau,[6] Robert Bingham,[8,9] Ian Shipsey,[1,*] Subir Sarkar,[1] and Gianluca Gregori[1]

[1]*Department of Physics, University of Oxford, Parks Road, Oxford OX1 3PU, United Kingdom*
[2]*Blackett Laboratory, Imperial College London, London SW7 2AZ, United Kingdom*
[3]*STFC, Rutherford Appleton Laboratory, Didcot OX11 0QX, United Kingdom*
[4]*Lawrence Berkeley National Laboratory, 1 Cyclotron Road, Berkeley, California 94720-8153, USA*
[5]*Max-Planck-Institut für Kernphysik Saupfercheckweg 1, 69117 Heidelberg, Germany*
[6]*European XFEL, Holzkoppel 4, 22869 Schenefeld, Germany*
[7]*Helmholtz-Zentrum Dresden-Rossendorf, Bautzner Landstraße 400, 01328 Dresden, Germany*
[8]*STFC, Rutherford Appleton Laboratory, Didcot OX11 0QX, United Kingdom*
[9]*John Anderson Building, University of Strathclyde, Glasgow G4 0NG, United Kingdom*

We present new exclusion bounds obtained at the European X-Ray Free Electron Laser facility (EuXFEL) on axionlike particles in the mass range 10^{-3} eV $\lesssim m_a \lesssim 10^4$ eV. Our experiment exploits the Primakoff effect via which photons can, in the presence of a strong external electric field, decay into axions, which then convert back into photons after passing through an opaque wall. While similar searches have been performed previously at a third-generation synchrotron [Yamaji *et al.*, Phys. Lett. B **782**, 523 (2018)], our work demonstrates improved sensitivity, exploiting the higher brightness of x-rays at EuXFEL.

Introduction—The axion arises from the breaking of Peccei-Quinn (PQ) symmetry [1–3], which was proposed to explain the absence of *CP* violation by the strong interactions described by quantum chromodynamics (QCD). Axionlike particles (ALPs) also arise in string theory [4]. In spite of being very light and having suppressed couplings, coherent oscillations of relic axions can naturally account for cold dark matter if $m_a \sim 10^{-6} - 10^{-4}$ eV [5–7]. Most laboratory searches for axions converting to photons in a magnetic field [8] have therefore focused on this "light axion window" [9], targeting axion-photon couplings corresponding to the Galactic halo dark matter being made of axions. This coupling is related (inversely) to the scale of PQ symmetry breaking in extensions of the standard model that implement the PQ symmetry, e.g., the Kim-Shifman-Vainshtein-Zakarov model [10,11] or the Dine-Fischler-Srednicki-Zhitnitsky (DFSZ) model [11,12]. It has been noted that when the PQ symmetry (in the DFSZ model) is broken after cosmological inflation, axions are also produced by the decay of domain walls [13], and the preferred mass for

axions to make up dark matter then exceeds 10^{-2} eV [14]. Such "heavy" axions are associated with a low scale of Peccei-Quinn symmetry breaking, so are theoretically preferred as being less susceptible to the "axion quality problem," namely, the potential destabilizing effects of quantum gravity on global symmetries [15–17].

Stringent bounds on such heavy axions (excluding astrophysical arguments derived from stellar cooling [18]) come from the CERN Axion Solar Telescope (CAST) [19]. This is a "helioscope" which looks for conversion of axions from the Sun into x-ray photons as they pass through a strong magnetic field. However, due to the specific experimental geometry of CAST, the axion-photon conversion probability gets highly suppressed for $m_a \gtrsim 1$ eV. For such masses, more competitive bounds arise from experiments which exploit Bragg conversion in the electric field of crystals, and underground searches for dark matter and $\beta\beta$ decay have been claimed to place strong bounds on the axion-photon coupling [20–27]. However, when the damping of x-rays in a crystal is taken into account, such bounds are considerably weakened [28]. Moreover, since the axions originate from the Sun there is necessarily some model dependence in extracting such bounds; the high plasma frequency and temperature on the Sun are particularly relevant as these can perturb the effective axion-photon coupling [18,29]. Similarly, bounds derived from stellar cooling arguments, e.g., neutrino observations of Supernova 1987a, have large astrophysical uncertainties [30].

---

*Deceased.

By contrast, in laboratory experiments the axion production process is directly controlled, avoiding such model dependence. Interesting constraints have been set by accelerator experiments, such as NOMAD [31], *BABAR* [32,33], and NA64 [34]. Laboratory-based searches for axions are thus well motivated even though they do not presently reach the same sensitivity as astrophysical limits. Of course, it is important to use as many different experimental approaches as is feasible, since each has its own characteristic strengths and limitations.

Here we present results from a new laboratory search for axions performed with the HED-HiBEF instrument at the European X-Ray Free Electron Laser (EuXFEL) in Hamburg [35]. This is sensitive to a broad range of axion and ALP mass between $\sim 10^{-3}$ and 10^4 eV. Our experiment exploits the Primakoff effect via which photons can decay into axions in the presence of a strong external electric field and then reconvert back into photons after passing through an opaque wall. This technique was previously employed in experiments with optical lasers and external magnetic fields [36–38].

When using x-rays, it is possible to increase the detection sensitivity by exploiting the electric fields which are present within a crystalline material. These atomic electric fields can be as high as 10^{11} V m^{-1} which, due to the form of the Hamiltonian, corresponds to magnetic field strengths of order 1 kT—much higher than the field strengths accessible using the best electromagnets. Although the length scales, which are accessible with crystal-based searches are smaller than for those with electromagnets, the path integrated equivalent field is competitive, being ~ 25 T m for the present study.

The strength of the effective magnetic field is calculated numerically using a Draic-Fock method [39,40]; these calculations are well verified experimentally, for example, in positron channeling experiments [41].

Furthermore, arranging atoms in a crystalline structure leads to a coherent effect analogous to Bragg scattering. Generation and reconversion can thus be carried out with a pair of x-ray crystals. This concept was first described by Buchmüller and Hoogeveen [42].

We improve on previous laboratory-based searches in the above mass range (up to which were performed using third-generation synchrotron facilities [43,44], but we achieve higher detection sensitivity due to the increased brightness of free electron lasers (FELs). This is because of the much shorter duration of the photon pulse which allows for a more accurate discrimination of the signal against the background.

Experimental setup—As discussed, a number of experiments have already placed bounds on the available axion parameter space, with varying degrees of model dependence. We use the term axion to describe both the QCD axion and any ALP which couples to photons via the dimension-five operator
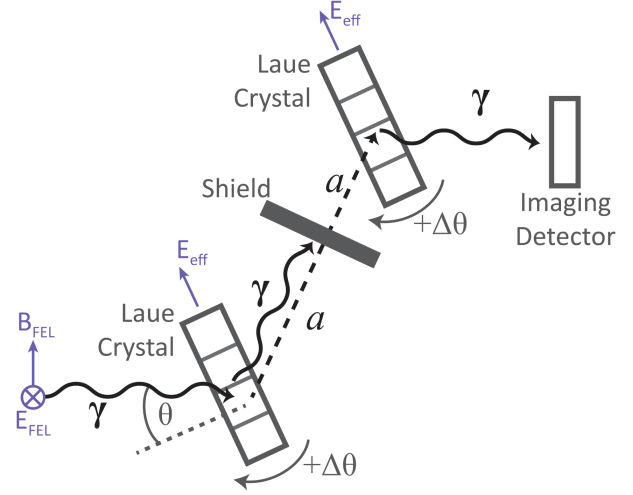

FIG. 1. Diagram of the setup in our experiment; the x-ray beam propagates from left to right. Here, $\mathbf{B}_{\text{FEL}}$ is the magnetic field in the XFEL beam, and $\mathbf{E}_{\text{eff}}$ is the crystalline electric field. Axion production and photon regeneration are expected to take place via the effective electric field within a pair of monolithic crystals, Ge (220) in Laue geometry, with dimensions $10 \times 10 \times 0.5$ mm^3. A pair of piezoelectric rotation stages (Xeryon, XRT-U30) were used to orient the germanium crystals. The shield is a 1 mm thick titanium sheet. The polarization of the x-ray beam maximizes the value of $\mathbf{B}_{\text{FEL}} \cdot \mathbf{E}_{\text{eff}}$ and thus the probability of axion production.

$$\mathcal{L}_{\text{axion}} = g_{a\gamma\gamma}\mathbf{E} \cdot \mathbf{B}a, \tag{1}$$

where $\mathbf{E} \equiv \mathbf{E}_{\text{eff}}$ is the electric field in the crystal lattice, $\mathbf{B} \equiv \mathbf{B}_{\text{FEL}}$ is the magnetic field associated with the electromagnetic wave of the x-ray photon, a is the *CP*-conserving scalar field of the axion, and $g_{a\gamma\gamma}$ is the axion-photon coupling. Note that here and throughout this Letter, unless otherwise noted, natural Heaviside-Lorentz units are used.

Experiments employing the above coupling exploit the Primakoff effect, viz., that there is a finite probability for a photon to decay into an axion in the presence of another photon, typically given by a static, external field. The conversion (or regeneration) probability is maximized when the electric and magnetic fields of these two photons are aligned. This probability increases linearly with the interaction length.

Our experimental setup is depicted in Fig. 1. It shows two germanium (Ge) crystals oriented in Laue geometry, with their lattice planes parallel to one another. The σ-polarized XFEL beam impinges on the first crystal from the left. The angle between the wave vector of the incoming x-ray beam and the lattice planes in the crystals is denoted θ. An important detail is that the Laue geometry is preferable to the more conventional Bragg scattering geometry because of the Borrmann effect, through which the transmission of x-rays in the Laue case is increased [42,44–46].

Both axions and Laue diffracted photons are transmitted through the first crystal. These are denoted, respectively, by a and γ in the figure. The photons are absorbed by a radiation shield, but the weakly interacting axions impinge on the second crystal. Here the strong electric field enables the regeneration of photons via the inverse Primakoff process. These regenerated photons are observed by a detector downstream of the crystals. In the configuration where $\theta = \theta_B$ (here, θ_B is the Bragg angle), the design is sensitive to a broad range of axion mass m_a satisfying the inequality

$$|m_a^2 - m_\gamma^2| \lesssim \frac{4k_\gamma}{L_{\text{eff}}}, \qquad (2)$$

where $m_\gamma = 44$ eV is the plasma frequency of the valence electrons in the conversion crystals [44], k_γ is the photon energy, and L_{eff} is the effective path length of x-rays within a crystal. We use units where $\hbar = c = 1$.

In the case where there is a detuning from the Bragg angle by $\Delta\theta = \theta - \theta_B$, it can be shown [44,46] that this setup becomes sensitive to a narrow range of axion mass ($\Delta m_a \sim 10^{-3}$ eV) centered on

$$m_a = \sqrt{m_\gamma^2 + 2q_T k_\gamma \cos(\theta_B)\Delta\theta}, \qquad (3)$$

where $q_T = 6.20$ keV is the magnitude of the reciprocal lattice vector. This means that by sweeping through different values of $\Delta\theta$, it is possible to search for heavy axions with mass in the interval between the plasma frequency of the crystal and the projection of the incoming photon energy onto the reciprocal lattice vector.

The EuXFEL was operated in a seeded mode, with 9.8 keV photon energy (wavelength, $\lambda_x = 2\pi/k_\gamma = 1.265$ Å). The repetition rate was 10 Hz, with one pulse per train. The x-ray beam was collimated by upstream compound refractive lenses. The full width at half maximum of the beam transverse profile was measured to be 400 μm at the center of the interaction chamber. The axion-photon conversion probability $P(a \leftrightarrow \gamma)$ for Laue-case diffraction is given by [44]

$$P(a \leftrightarrow \gamma) = \left(\frac{1}{4} g_{a\gamma\gamma} E_{\text{eff}} L_{\text{eff}} \cos\theta_B\right)^2, \qquad (4)$$

where $E_{\text{eff}} = 7.3 \times 10^{10}$ V m^{-1} is the crystalline electric field [44] and

$$L_{\text{eff}} = 2L_{\text{att}}^B\left(1 - e^{-L_x/2L_{\text{att}}^B}\right), \qquad (5)$$

where $L_x = \ell/\cos(\theta_B + \Delta\theta)$ is the x-ray path length inside the crystals ($\ell = 500$ μm is the thickness of each crystal) and $L_{\text{att}}^B = 1499.8$ μm (for σ polarization) [47].

TABLE I. Summary of the different runs which were performed during the experiment. The detuning angles $\Delta\theta$, corresponding masses m_a, total number of photons incident upon the apparatus N_{in}, and inferred bound on the strength of the axion-photon coupling constant $g_{a\gamma\gamma}$ are indicated.

$\Delta\theta$ (mrad)	m_a (eV)	N_{in} ($\times 10^{16}$)	$g_{a\gamma\gamma}$ (GeV^{-1})
0.0	$\lesssim 44$	2.6	3.91×10^{-4}
1.0	3.4×10^2	2.4	3.10×10^{-4}
1.8	4.6×10^2	1.6	3.87×10^{-4}
10.0	1.1×10^3	1.7	3.69×10^{-4}
50.0	2.4×10^3	1.5	2.76×10^{-4}

Since the x-ray pulse duration in our experiment is short compared to that at a synchrotron facility, the result presented above requires a modification. For a short (i.e., transform-limited) x-ray pulse, the width of the rocking curve ($\Delta\theta_{\text{RC}}$) and timescale of the scattering process (Δt) form a time-bandwidth product given by [48,49]

$$\Delta\theta_{\text{RC}}\Delta t \simeq \frac{\lambda_x \tan\theta_B}{c}, \qquad (6)$$

where for clarity we have reinstated c, the speed of light.

Because of the Borrmann effect, the extinction length of the x-rays is longer than the x-ray path length in the crystal, and therefore, the characteristic timescale is simply given by the geometric time delay due to scattering off multiple planes,

$$c\Delta t = 2\ell \tan\theta_B \sin\theta_B. \qquad (7)$$

Combining these two expressions yields a rocking curve width $\Delta\theta_{\text{RC}} \simeq 0.4$ μrad, which is far narrower than the Darwin width $\Delta\theta_D = 44$ μrad for Ge (220) [50]. By the rocking curve width, we mean the actual angular spread in incoming x-rays which are transmitted through the crystal. Meanwhile, the Darwin width refers to the predicted angular spread obtained with a theory that neglects time dependence.

As shown in Ref. [44], the effective conversion length is inversely proportional to the width of the rocking curve. However, in deriving Eq. (4), it was assumed that the Darwin width and rocking curve width were equivalent. This narrowing of the rocking curve may also be interpreted as a change in the effective index of refraction inside the crystal lattice. Following the same steps as in Ref. [44], it can then be readily shown that the interaction amplitude must increase by a factor $\xi_B = \Delta\theta_D/\Delta\theta_{\text{RC}}$. Thus, the scattering probability becomes

$$P(a \leftrightarrow \gamma) \simeq \left(\frac{1}{4} g_{a\gamma\gamma} E_{\text{eff}} L_{\text{eff}} \xi_B \cos\theta_B\right)^2. \qquad (8)$$
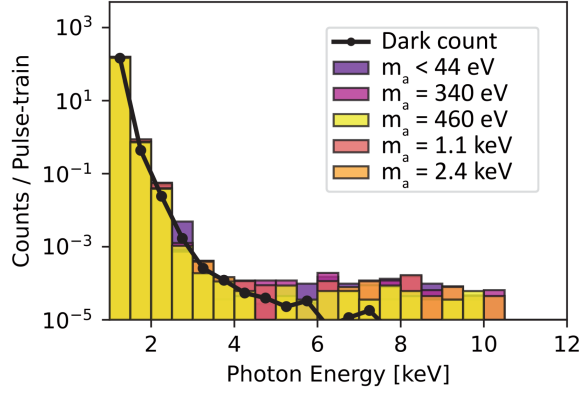
FIG. 2. A histogram showing the events detected across all acquisitions and over the whole detector area. The number of counts in a 24 hour dark run are also shown.
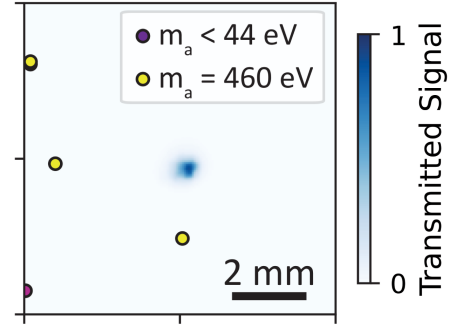

FIG. 3. An image showing the transmitted signal in the absence of the radiation shield (blue color map) overlaid with the position of $k_\gamma \geq 4$ keV events across all data acquisitions. A fiducial indicating scale on the detector plane is also shown.

While an exact derivation of this result would require a full solution of the time-dependent dynamical diffraction equations, as outlined in Ref. [48], the above expression is accurate to within a factor of order unity.

Results—The regenerated photons were measured using a silicon hybrid-pixel JUNGFRAU detector [51]. Further details regarding data acquisition and the steps taken to ensure alignment stability are provided in Supplemental Material [52].

Our search was limited to five discrete $\Delta\theta$ values, with data collected for 60–90 min at each angle. Table I shows the bounds on the axion-photon coupling determined from our data at each detuning angle.

Figure 2 is a histogram which shows energy-resolved events for each of the datasets which are detailed in Table I. These are compared against the number of counts in a 24-hour-long dark run. ALP observations can be distinguished from the background as reconverted x-rays must be identical to the primary EuXFEL x-rays, and moreover must fall inside the region on the detector which is impacted by the x-ray beam when the shield is absent.

To establish if any of the few events in the relevant energy band do fall upon the x-ray spot and might therefore be associated with axion production, hit maps of events were produced as in Fig. 3. The blue color map shows transmission through the setup in the absence of the radiation shield, while the overlaid data points indicate the location of hits on the detector with a photon energy exceeding 4 keV for each of the datasets in Table I.

As Fig. 3 shows, there are no events which overlap with the region of the x-ray spot (the darker blue region in the center of the figure). Their absence implies that no events consistent with axion production were detected during the experiment. The corresponding limit on the axion-photon coupling is then obtained by inverting Eq. (8):

$$g_{a\gamma\gamma} < \left(\frac{1}{4}E_{\text{eff}}L_{\text{eff}}\xi_B \cos\theta_B\right)^{-1} P(a \leftrightarrow \gamma)^{1/2}, \quad (9)$$

with $P(a \leftrightarrow \gamma)^2 = (N_{\text{det}}/\eta N_{\text{in}})$, N_{det} is the detected number of photons, and N_{in} is the number of input photons.

The efficiency factor η accounts for losses associated with the deviation from parallelism between the two crystals, fluctuations in the exact x-ray energy, and the quantum efficiency of the detector. The value of η was obtained experimentally: At the beginning and end of each data run, the crystals were tuned to the Bragg angle, and the radiation shield was removed in order to characterize the experimental setup. During these characterization phases, the efficiency factor for the ith run at a given detuning angle η_i was given by

$$\eta_i = \frac{1}{T_{\text{Ge}}^2}\frac{E_i^{\text{JF,ch}}}{E_{i/}^{\text{in,ch}}}, \quad (10)$$

where T_{Ge} is the transmission factor associated with a single crystal, $E_i^{\text{JF,ch}}$ is the total x-ray dose measured on the (downstream) JUNGFRAU detector during these characterization phases, and $E_i^{\text{in,aq}}$ is the total x-ray dose measured (during characterization) on a passive upstream monitor [53].
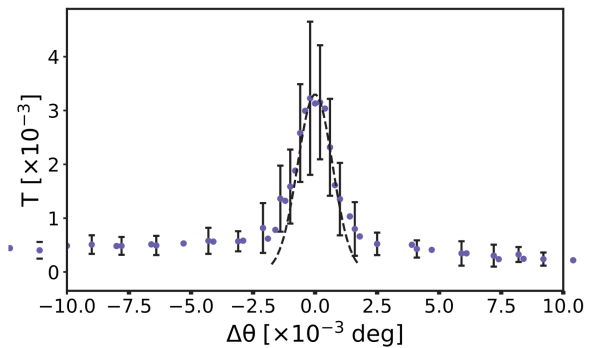

FIG. 4. X-ray transmission through a single Ge crystal as a function of the detuning angle $\Delta\theta$. The central peak is fitted with a Gaussian (dashed line) of width $\Delta\theta_s \approx 17.4$ µrad. An average of 145 shots per angular point are used to construct the peak curve, while 32 shots are used for each angular point on the baseline. The error bars on the measurements are 1σ.
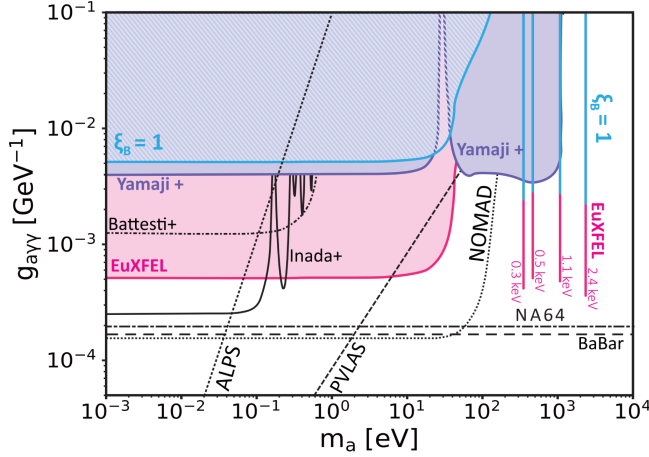
FIG. 5. Bounds on the axion-photon coupling from our experiment (pink) compared with those from Yamaji *et al.* [43,44] (purple). The excluded region (blue) taking $\xi_B = 1$ in Eq. (9) is also shown to illustrate the improvement due to the higher photon number. Shown for comparison are bounds from other laboratory searches: NOMAD [31], PVLAS [56], ALPS [37], NA64 [34], BABAR [32,33], Battesti *et al.* [57], and Inada *et al.* [58]. To aid visualization, the width of the off-Bragg bounds inferred from our search (in reality, only $\sim 10^{-3}$ eV) is exaggerated here. The masses associated with off-Bragg searches are also labeled in the figure.

Because of the very narrow rocking curve for Laue-case diffraction, a single Ge crystal can be used to determine the EuXFEL spectral profile by detuning it from the Bragg angle and recording the transmitted intensity on a separate JUNGFRAU detector as a function of the detuning angle. This is shown in Fig. 4, where the seeded x-ray beam is shown to have an energy bandwidth of $\Delta E/E = \Delta\theta_s/\tan\theta_B = 5.2 \times 10^{-5}$ or ~ 0.5 eV at 9.8 keV. This is indeed expected for a self-seeded beam [54], and the variations in the transmitted intensity are associated with shot-to-shot variability in the exact seeded pulse energy. Overall, the transmission through a single crystal is determined to be of order $T_{\mathrm{Ge}} \approx 3 \times 10^{-3}$.

For the data collection phases of a given dataset, the value of ηN_{in} was then taken to be

$$\eta N_{\mathrm{in}} = \sum_i \eta_i E_i^{\mathrm{in,aq}}/k_\gamma, \qquad (11)$$

where the summation is across all runs at a given detuning angle, $E_i^{\mathrm{in,aq}}$ is the dose measured on the passive upstream monitor during data collection, and $k_\gamma = 9.8$ keV is the photon energy. To obtain a 90% CL upper bound based on the observation of zero events consistent with axion production, we then take $N_{\mathrm{det}} = 2.3$ events [55].

Concluding remarks—The outcome of this analysis of data collected at EuXFEL is shown in Fig. 5, which summarizes bounds in the meV–few keV mass range,

from searches for laboratory-generated axions. We were able to improve on the results from Ref. [43] at several discrete axion masses.

For $m_a \gtrsim 200$ eV, we are able achieve a sensitivity within a factor 10 of the most competitive previous searches, namely, NA64 [34] and BABAR [32,33]. Although our search is presently not as sensitive as these experiments, our result constitutes an important validation, especially as the NA64 and BABAR limits were extracted assuming different production and detection mechanisms for axions, namely, spontaneous axion decay and/or flavor-changing meson decay, rather than the Primakoff process as in our case.

We emphasize that this is not the best sensitivity achievable with the present setup. Issues with x-ray heating forced us to attenuate the x-ray flux by a factor of 10^3. Moreover, the x-ray bunch structure was set with the number of pulses per train limited to one, out of a possible 300. Issues with retaining alignment also limited data acquisition time to 60–90 min at each detuning angle; with a more stable setup that would include active cooling of the first conversion crystal, these times could be increased by a factor of 30. Furthermore, we could also fully exploit the Borrmann effect and use Ge crystals up to 1.5 mm in thickness. Taken together, these improvements would increase the sensitivity by a factor ~ 150, bringing the estimated bounds down to 2×10^{-6} GeV^{-1}, close to the expectation for QCD axions to be dark matter [59]. Below ~ 1 eV, these bounds are also comparable to proposed photon regeneration experiments using superconducting pulsed magnetic fields [60]. Currently, no experiment has the level of sensitivity for $m_a \gtrsim 10$ eV that we anticipate for future searches with the platform described here.

Data availability—The raw data recorded for this experiment at the European XFEL are available [61].

[1] R. D. Peccei and H. R. Quinn, *CP* conservation in the presence of instantons, Phys. Rev. Lett. **38**, 1440 (1977).

[2] S. Weinberg, A new light boson?, Phys. Rev. Lett. **40**, 223 (1978).

[3] F. Wilczek, Problem of strong *P* and *T* invariance in the presence of instantons, Phys. Rev. Lett. **40**, 279 (1978).

[4] P. Svrcek and E. Witten, Axions in string theory, J. High Energy Phys. 06 (2006) 051.

[5] J. Preskill, M. B. Wise, and F. Wilczek, Cosmology of the invisible axion, Phys. Lett. **120B**, 127 (1983).

[6] L. F. Abbott and P. Sikivie, A cosmological bound on the invisible axion, Phys. Lett. **120B**, 133 (1983).

[7] M. Dine and W. Fischler, The not so harmless axion, Phys. Lett. **120B**, 137 (1983).

[8] P. Sikivie, Experimental tests of the invisible axion, Phys. Rev. Lett. **51**, 1415 (1983); **52**, 695(E) (1984).

[9] Y. K. Semertzidis and S. Youn, Axion dark matter: How to see it?, Sci. Adv. **8**, abm9928 (2022).

[10] J. E. Kim, Weak interaction singlet and strong *CP* invariance, Phys. Rev. Lett. **43**, 103 (1979).

[11] M. Dine, W. Fischler, and M. Srednicki, A simple solution to the strong *CP* problem with a harmless axion, Phys. Lett. **104B**, 199 (1981).

[12] A. R. Zhitnitsky, On possible suppression of the axion hadron interactions. (In Russian), Sov. J. Nucl. Phys. **31**, 260 (1980).

[13] A. Ringwald and K. Saikawa, Axion dark matter in the post-inflationary Peccei-Quinn symmetry breaking scenario, Phys. Rev. D **93**, 085031 (2016); **94**, 049908(E) (2016).

[14] K. A. Beyer and S. Sarkar, Ruling out light axions: The writing is on the wall, SciPost Phys. **15**, 003 (2023).

[15] M. Kamionkowski and J. March-Russell, Planck scale physics and the Peccei-Quinn mechanism, Phys. Lett. B **282**, 137 (1992).

[16] R. Holman, S. D. H. Hsu, T. W. Kephart, E. W. Kolb, R. Watkins, and L. M. Widrow, Solutions to the strong *CP* problem in a world with gravity, Phys. Lett. B **282**, 132 (1992).

[17] S. M. Barr and D. Seckel, Planck scale corrections to axion models, Phys. Rev. D **46**, 539 (1992).

[18] A. Caputo and G. Raffelt, Astrophysical axion bounds: The 2024 Edition, Proc. Sci. COSMICWISPers (2024) 041 [arXiv:2401.13728].

[19] V. Anastassopoulos *et al.* (CAST Collaboration), New CAST limit on the axion-photon interaction, Nat. Phys. **13**, 584 (2017).

[20] F. T. Avignone III, D. Abriola, R. L. Brodzinski, J. I. Collar, R. J. Creswick, D. E. DiGregorio, H. A. Farach, A. O. Gattone, C. K. Guerard, F. Hasenbalg, H. Huck, H. S. Miley, A. Morales, J. Morales, S. Nussinov, A. OrtizdeSolorzano, J. H. Reeves, J. A. Villar, and K. Zioutas (SOLAX Collaboration), Experimental search for solar axions via coherent Primakoff conversion in a germanium spectrometer, Phys. Rev. Lett. **81**, 5068 (1998).

[21] R. Bernabei *et al.*, Search for solar axions by Primakoff effect in NaI crystals, Phys. Lett. B **515**, 6 (2001).

[22] A. Morales *et al.* (COSME Collaboration), Particle dark matter and solar axion searches with a small germanium detector at the Canfranc Underground Laboratory, Astropart. Phys. **16**, 325 (2002).

[23] Z. Ahmed *et al.* (CDMS Collaboration), Search for axions with the CDMS experiment, Phys. Rev. Lett. **103**, 141802 (2009).

[24] P. Belli, R. Bernabei, F. Cappella, R. Cerulli, F. A. Danevich, A. Incicchitti, V. V. Kobychev, M. Laubenstein, O. G. Polischuk, and V. I. Tretyak, Search for Li-7 solar axions using resonant absorption in LiF crystal: Final results, Phys. Lett. B **711**, 41 (2012).

[25] E. Armengaud *et al.*, Axion searches with the EDELWEISS-II experiment, J. Cosmol. Astropart. Phys. 11 (2013) 067.

[26] I. J. Arnquist *et al.* (Majorana Collaboration), Search for solar axions via axion-photon coupling with the Majorana demonstrator, Phys. Rev. Lett. **129**, 081803 (2022).

[27] E. Aprile *et al.* (XENON Collaboration), Search for new physics in electronic recoil data from XENONnT, Phys. Rev. Lett. **129**, 161805 (2022).

[28] J. B. Dent, B. Dutta, and A. Thompson, Bragg-Primakoff axion photoconversion in crystal detectors, arXiv:2307.04861.

[29] J. Jaeckel, E. Masso, J. Redondo, A. Ringwald, and F. Takahashi, The need for purely laboratory-based axion-like particle searches, Phys. Rev. D **75**, 013004 (2007).

[30] N. Bar, K. Blum, and G. D'Amico, Is there a supernova bound on axions?, Phys. Rev. D **101**, 123025 (2020).

[31] P. Astier *et al.* (NOMAD Collaboration), Search for eV (pseudo)scalar penetrating particles in the SPS neutrino beam, Phys. Lett. B **479**, 371 (2000).

[32] J. P. Lees *et al.* (*BABAR* Collaboration), Search for invisible decays of a dark photon produced in e^+e^- collisions at *BABAR*, Phys. Rev. Lett. **119**, 131804 (2017).

[33] M. J. Dolan, T. Ferber, C. Hearty, F. Kahlhoefer, and K. Schmidt-Hoberg, Revised constraints and Belle II sensitivity for visible and invisible axion-like particles, J. High Energy Phys. 12 (2017) 094; 03 (2021) 190(E).

[34] D. Banerjee *et al.* (NA64 Collaboration), Search for axion-like and scalar particles with the NA64 experiment, Phys. Rev. Lett. **125**, 081801 (2020).

[35] U. Zastrau, K. Appel, C. Baehtz, O. Baehr, L. Batchelor, A. Berghäuser, M. Banjafar, E. Brambrink, V. Cerantola, T. E. Cowan *et al.*, The high energy density scientific instrument at the European XFEL, J. Synchrotron Radiat. **28**, 1393 (2021).

[36] C. Robilliard, R. Battesti, M. Fouche, J. Mauchain, A.-M. Sautivet, S. Faure, M. Nardone, J. L. Paillard, F. Amiranoff, and C. Rizzo, No light shining through a wall, Phys. Rev. Lett. **99**, 190403 (2007).

[37] K. Ehret *et al.*, New ALPS results on hidden-sector lightweights, Phys. Lett. B **689**, 149 (2010).

[38] R. Ballou *et al.* (OSQAR Collaboration), New exclusion limits on scalar and pseudoscalar axionlike particles from light shining through a wall, Phys. Rev. D **92**, 092002 (2015).

[39] P. A. Doyle and P. S. Turner, Relativistic Hartree–Fock X-ray and electron scattering factors, Acta Cryst. **A24**, 390 (1968).

[40] V. N. Baier, V. M. Katkov, and V. Strakhovenko, *Electromagnetic Processes at High Energies in Oriented Single Crystals* (World Scientific, Singapore, 1998).

[41] M. Atkinson, J. Bak, P. Bussey, P. Christensen, J. Ellison, R. Ellison, K. Eriksen, D. Giddings, R. Hughes-Jones,

B. Marsh, D. Mercer, F. Meyer, S. Møller, D. Newton, P. Pavlopoulos, P. Sharp, R. Stensgaard, M. Suffert, and E. Uggerhøj, Radiation from planar channeled 5–55 solgevc positrons and elctrons, Phys. Lett. B **110**, 162 (1982).

[42] W. Buchmuller and F. Hoogeveen, Coherent production of light scalar particles in Bragg scattering, Phys. Lett. B **237**, 278 (1990).

[43] T. Yamaji, K. Tamasaku, T. Namba, T. Yamazaki, and Y. Seino, Search for axion like particles using Laue-case conversion in a single crystal, Phys. Lett. B **782**, 523 (2018).

[44] T. Yamaji, T. Yamazaki, K. Tamasaku, and T. Namba, Theoretical calculation of coherent Laue-case conversion between X-rays and ALPs for an X-ray light-shining-through-a-wall experiment, Phys. Rev. D **96**, 115001 (2017).

[45] E. K. Kovev, O. N. Efimov, and L. I. Korovin, Characteristics of anomalous transmission of X-rays in the general case of laue diffraction, Phys. Status Solidi (b) **35**, 455 (1969).

[46] W. Liao, Generation and search of axion-like light particle using intense crystalline field, Phys. Lett. B **702**, 55 (2011).

[47] From https://x-server.gmca.aps.anl.gov/x0h.html.

[48] J. Wark and R. Lee, Simulations of femtosecond X-ray diffraction from unperturbed and rapidly heated single crystals, J. Appl. Crystallogr. **32**, 692 (1999).

[49] Y. Shvyd'ko and R. Lindberg, Spatiotemporal response of crystals in X-ray Bragg diffraction, Phys. Rev. ST Accel. Beams **15**, 100702 (2012).

[50] From https://x-server.gmca.aps.anl.gov/x0h.html.

[51] A. Mozzanica, A. Bergamaschi, M. Brueckner, S. Cartier, R. Dinapoli, D. Greiffenberg, J. Jungmann-Smith, D. Maliakal, D. Mezza, M. Ramilli, C. Ruder, L. Schaedler, B. Schmitt, X. Shi, and G. Tinti, Characterization results of the JUNGFRAU full scale readout ASIC, J. Instrum. **11**, C02047 (2016).

[52] See Supplemental Material at http://link.aps.org/supplemental/10.1103/PhysRevLett.134.055001 for a description of experimental data collection and methods.

[53] T. Maltezopoulos, F. Dietrich, W. Freund, U. F. Jastrow, A. Koch, J. Laksman, J. Liu, M. Planas, A. A. Sorokin, K. Tiedtke, and J. Grünert, Operation of X-ray gas monitors at the European XFEL, J. Synchrotron Radiat. **26**, 1045 (2019).

[54] C. Emma, A. Lutman, M. W. Guetg, J. Krzywinski, A. Marinelli, J. Wu, and C. Pellegrini, Experimental demonstration of fresh bunch self-seeding in an X-ray free electron laser, Appl. Phys. Lett. **110**, 154101 (2017).

[55] T. Junk, Confidence level computation for combining searches with small statistics, Nucl. Instrum. Methods Phys. Res., Sect. A **434**, 435 (1999).

[56] F. Della Valle, A. Ejlli, U. Gastaldi, G. Messineo, E. Milotti, R. Pengo, L. Piemontese, G. Ruoso, and G. Zavattini, New PVLAS model independent limit for the axion coupling to $\gamma\gamma$ for axion masses above 1 meV, in *10th Patras Workshop on Axions, WIMPs and WISPs* (2014), pp. 67–70, arXiv:1410.4081.

[57] R. Battesti, M. Fouche, C. Detlefs, T. Roth, P. Berceau, F. Duc, P. Frings, G. L. J. A. Rikken, and C. Rizzo, A photon regeneration experiment for axionlike particle search using X-rays, Phys. Rev. Lett. **105**, 250405 (2010).

[58] T. Inada *et al.*, Search for two-photon interaction with axionlike particles using high-repetition pulsed magnets and synchrotron X rays, Phys. Rev. Lett. **118**, 071803 (2017).

[59] C. A. J. O'Hare, Cosmology of axion dark matter, Proc. Sci. COSMICWISPers(2024) 040 [arXiv:2403.17697].

[60] R. Rabadan, A. Ringwald, and K. Sigurdson, Photon regeneration from pseudoscalars at X-ray laser facilities, Phys. Rev. Lett. **96**, 110407 (2006).

[61] 10.22003/XFEL.EU-DATA-003326-00